Process Safety and Environmental Protection 136 (2020) 49–55

Contents lists available at ScienceDirect

Process Safety and Environmental Protection

journal homepage: www.elsevier.com/locate/psep

Agent-Based model to predict the fate of the degradation of organic compounds in the aqueous-phase UV/H_2O_2 advanced oxidation process

Robert Zupko [a], Divya Kamath [b], Erica Coscarelli [b], Mark Rouleau [a], Daisuke Minakata [b,*]

[a] Department of Social Sciences, Michigan Technological University, 1400 Townsend Drive, Houghton, MI, 49931, USA
[b] Department of Civil and Environmental Engineering, Michigan Technological University, 1400 Townsend Drive, Houghton, MI, 49931, USA

ARTICLE INFO

Article history:
Received 10 December 2019
Received in revised form 14 January 2020
Accepted 15 January 2020
Available online 23 January 2020

Keywords:
Agent-based modeling
UV/H_2O_2 advanced oxidation process
Fate of acetone degradation

ABSTRACT

Advanced oxidation processes (AOPs) are promising water treatment technologies used to destroy trace organic compounds. Yet, the inability to predict the degradation fate of trace organic compounds due to their diverse chemical structures and potential for transformation byproducts greatly limits AOP effectiveness. Current prediction methods are time consuming and discontinuous because they rely on conventional kinetic models that often require solving 'stiff' ordinary differential equations numerically. In this study, we present a novel approach to AOP degradation prediction that uses an agent-based model to represent the chemical entities of individual molecular species and to simulate the movement and reactions of these entities over time in a defined space. Predicted time-dependent concentration profiles of a parent test compound, acetone, and its transformation products in UV/H_2O_2 AOP are shown to be consistent with our experimental observations.

1. Introduction

Insufficient removal of trace organic compounds is a common and significant problem for conventional water treatment technologies. (Westerhoff et al., 2005) This problem causes an alarmingly wide range of harmful compounds to flow into both natural waterways and water/wastewater treatment processes (Kolpin et al., 2002; Heidler and Halden, 2008). The persistence of such contaminants in waterways then raises public concern over uncertain toxicological risks to human health and natural ecosystems (Heyes et al., 2010). It is for these reasons that there is a growing need to predict the fate of trace organic compounds to ensure their full attenuation in the treatment process, which is then compounded by expected increases in de facto and planned water reuse as well as the continual identification of more trace organic compounds over time. (NRC, 2012)

Advanced oxidation processes (AOPs) that produce highly reactive radical species at ambient temperature and atmospheric pressure are promising technologies for the degradation of trace organic compounds in water. (Glaze et al., 1987; Glaze and Kang, 1989) Within an AOP, electrophiles, such as hydroxyl radicals ($HO^{\bullet}$), react with the electron rich sites of an organic compound to destroy it via radical-involved chain reactions. (Buxton et al., 1988) Several kinetic models have been developed to predict the degradation fate of organic compounds in AOPs based upon experimentally identified reaction pathways and reaction rate constants (Guo et al., 2014; Crittenden et al., 1999). Our own research has recently identified more than 200 elementary reaction pathways for $HO^{\bullet}$-induced acetone degradation in a UV/H_2O_2 AOP and predicted their reaction rate constants using *ab initio* quantum mechanical calculations. (Kamath et al., 2018) This work required numerically solving a set of ordinary differential equations (ODEs) for each reaction species to produce time-dependent concentration profiles of a parent organic compound and its degradation byproducts. Yet, differences in species concentrations and reaction rate constants by more than several orders of magnitude in AOPs result in 'stiff' differential equations that are challenging to solve numerically and may require as much as 10^8-10^{12} steps in each of the hundreds of governing equations to replicate what occurs in engineered treatment systems in just minutes (Peyton, 1990). Thus, there is a pressing need for alternative prediction methods to conventional kinetic models that are not tied to ODEs.

Agent-based model (ABM) offers a novel alternative to conventional kinetic models that makes it possible to simulate chemical reactions at the level of individual species (i.e., radicals and organic compounds) to predict the byproduct-fate of trace organic com-

* Corresponding author.
E-mail address: dminakat@mtu.edu (D. Minakata).

https://doi.org/10.1016/j.psep.2020.01.023
0957-5820/

pounds without having to numerically solve 'stiff' ODEs. Unlike ODE-based models, ABMs can simulate any number or relative distribution of reactants in three-dimensional space over time while allowing for competitive reactions that produce different byproducts simultaneously. These features enable ABMs to overcome the limitations of 'stiff' ODEs that are challenging to solve, require large amounts of time to derive a solution, and can result in volatile solutions between interdependent differential equations. It is for these reasons that ABMs have already been applied to a variety of biological systems with mechanistic insights inside the cell (Pogson et al., 2006; Bachman and Sorger, 2011; Klann et al., 2011).

In this study, we demonstrate how ABM simulation can be used to predict byproduct concentration profiles based upon the degradation of a test compound, acetone, in UV/H_2O_2 AOP. We also perform a bench-top photochemical experiment and compare the time-dependent concentration profiles of acetone and its degradation products against our ABM concentration profiles to validate our findings. Limitations of the ABM approach and environmental implications are also discussed.

2. Materials and methods

2.1. Experiments

A benchtop photoreactor was used to perform UV/H_2O_2 AOP for a test target compound, acetone. The photoreactor was comprised of a 1.8 L Wheaton Roller and a low pressure Atlantic UV lamp with a wavelength of 254 nm, based upon the spectral distribution provided for the lamp by Ace Glass Inc. A quartz immersion well was used to circulate water around the lamp to prevent overheating and reactor vessels were surrounded by circulating water to maintain a constant temperature. The entire photoreactor was contained in a glass box covered by aluminum foil to prevent the escape of UV light. Each reactor vessel was equipped with a magnetic stir plate and stir rod to ensure that completely mixed conditions were maintained and a dye study was conducted to verify the conditions. During experiments the desired organic compound and H_2O_2 were added to the reactor vessels and sampled at desired time steps. Samples were placed in amber vials when drawn and stored at 4 °C until they were analyzed using gas chromatography, high performance liquid chromatography, and ion chromatography.

ACS grade chemicals were obtained from Sigma-Aldrich for both the experimental solutions (acetone and hydrogen peroxide) and stock solutions (oxalic acid, formic acid, acetic acid, glyoxylic acid, pyruvaldehyde 40 % weight in solution, and pyruvic acid); along with formaldehyde from Fisher Scientific. Experimental solutions were prepared using MilliQ water (resistance > 18.2 MΩ.cm) obtained from a Millipore purification system and 10 mM hydrogen peroxide to 1 mM of acetone along with parachloro benzoic acid (pCBA) solution, 0.25 μM, was also added as a probe compound for hydroxyl radicals. Stock solutions were made for desired concentrations and diluted to create standard solutions in the anticipated concentration range for calibration curves.

Light intensity in the reactor was measured to be 5.16×10^{-7} Einstein/L-s using ferrioxalate actinometry and temperature controls kept the photoreactor within ±1 °C of the initial temperature. As a result, kinetics were observed to be those occurring at room temperature. Acetone, formaldehyde, and pyruvic aldehyde were measured via derivatization with 2,4-dinitrophenyl hydrazine followed by analyses using a UHPLC 2000 series Dionex equipped with a reverse phase C-18 column (4.5 mm x 250 mm) using acetonitrile and water in a gradient flow condition at 0.8 mL/min as the mobile phase. Retention times for formaldehyde, acetone, and pyruvate were 10.1 min, 21.1 min, and 14 min, respectively using this method. Concentrations of pCBA were also determined using this system and reverse phase HPLC with a C-18 column although a different eluent with 45 % of acetonitrile and 55 % of 10 mM H_3PO_4 was used to find a retention time of 7.8 min at a 254 nm wavelength for pCBA. To determine the concentration of hydrogen peroxide, 2,9-dimethyl-1,10-phenanthroline (DMP) method was used for a diluted sample to ensure that concentrations were within the valid μM range. Ion chromatography with a Dionex ICS 2100 series equipped with an ion-exchange column was used to determine concentration of organic anions, acetate, formate, pyruvate and oxalate. Finally, total organic carbon (TOC) was determined using a TOC analyzer, GE sievers.

2.2. Agent-based model

2.2.1. Model development

Chemical species in our ABM are simulated as single entities or agents capable of moving and reacting with other reactant agents within the space of a simulated photo-reactor. At simulation start, one agent is created for every chemical species and then randomly distributed in our simulated reactor space to replicate a completely mixed batch photo-reactor. Each agent then randomly moves through space based upon Brownian motion until colliding with another potential reactant agent to produce a byproduct agent up to the point at which the species is exhausted or the simulation ends.

Reactions of agents of two or more different chemical species sharing the same simulated reactor space with corresponding reaction kinetics that are in agreement take place in our ABM as follows. Given a generic reaction A + B → C at the second order reaction rate constant of k, if the chemical entity B is within an interaction space, v_a, in a spherical shape, the chemical entity A can interact with the entity B. The change in the concentration of A, $C_a(t)$, over a specified time can be expressed using the concentration, $C_b(t)$, of species B at time t.

$$\frac{dC_a(t)}{dt} = -kC_a(t)C_b(t) \tag{1}$$

Given that the magnitude of the change in concentration of A during a time interval of Δt is ΔC_a, the concentration of A at time $t + \Delta t$ can be given as

$$C_a(t+\Delta t) = C_a(t) - \Delta C_a \tag{2}$$

When Δt becomes sufficiently small, ΔC_a is assumed to be equal to

$$\Delta C_a \approx -\Delta t \frac{dC_a(t)}{dt} \tag{3}$$

Using the relationships between Eqs (1) and (3), ΔC_a can be written as

$$\Delta C_a = kC_a(t)C_b(t)\Delta t \tag{4}$$

Considering the stoichiometric coefficients of the given reaction, the proportion of B molecules that interact with A at each time interval can be written as

$$\frac{\Delta C_b}{C_b(t)} = \frac{\Delta C_a}{C_b(t)} = kC_a(t)\Delta t \tag{5}$$

Because the proportional ratio above holds for the total volume, V, (m^3) inside which A interacts with B, the total volume inside which A interacts with B, V_a, is given as

$$V_a = kC_a(t)\Delta tV \tag{6}$$

In the reaction between A and B, if the chemical entity B is within an interaction space, v_a, in a spherical shape, the chemical entity A

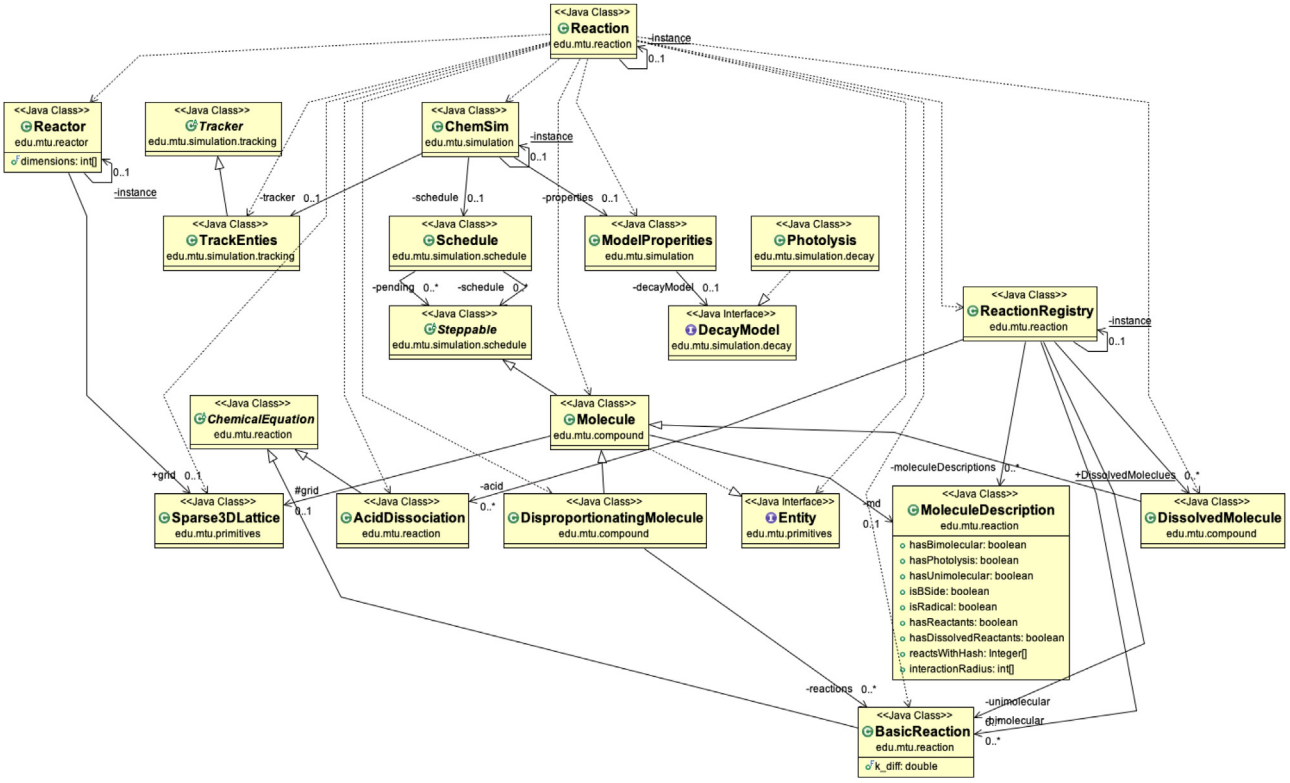

Fig. 1. Overall procedure of agent-based model.

can interact with the entity B. The interaction space can be written as

$$v_a = \frac{V_a}{n_a(t)} = \frac{kC_a(t)\Delta tV}{C_a(t)N_aV} = \frac{k\Delta t}{N_a} \tag{7}$$

where, $n_a(t)$ is the number of molecules A at any time, and N_a is the Avogadro numbers, 6.02×10^{23} molecules/mole. The maximum radius of the interaction space can be calculated as

$$r = \sqrt[3]{\frac{3k\Delta t}{4\pi N_a}} \tag{8}$$

While this radius may be interpreted as a crisp boundary as shown in Pogson et al. (2006) (Pogson et al., 2006), we introduced a probability for each reaction that uses a Gaussian error function to replicate the increased likelihood of a reaction occurring as the distance between reactant entities decreases.

2.2.2. Procedure of agent-based model simulation

Model initialization requires two input files: (1) a file specifying the model's starting conditions (i.e., reactor size, UV/H_2O_2 photolysis rate, a parent chemical entity, concentrations, p*K*a of chemical entities and reactions) and (2) a file listing the complete reaction pathway to identify potential reactant agents and their expected byproducts. A reaction registry is then used to store the list of possible chemical reactions and to manage these reactions once they occur in the simulated reactor as specified above. Prior to the start of photochemical reactions, molar concentrations of a target chemical species and H_2O_2 provided in the input file are converted to a count of chemical entities by a statistical normalization

$$N_i = \left(n_i / \sum_{i=1}^{N} n_i \right) \times N \tag{9}$$

Once initialization is complete, the model simulates photochemical reactions for the designated number of time steps specified in the initialization file. A scheduler is used to activate chemical entities individually, once each time step, to allow movement and chemical reactions to take place. The scheduler uses a deque array backed by a list array to activate entities each time step in a manner that allows for constant time insertion and retrieval as well as a variable number of chemical entities. A Fisher-Yates shuffle is used to randomly order the list array that is copied to the deque array at the beginning of the current time step. Chemical entities are then popped from the dequeue array to execute their movement and reaction operations so long as that entity has not been involved in a prior reaction in the current time step. The entity is then flagged to signal step completion until the next round to ensure proper execution of parallel reactions. Upon exhaustion of the deque array (i.e., the end of a time step), the list array is then re-shuffled and copied to the deque array to begin the next time step.

Brownian motion is used to simulate the movement or diffusion of the chemical entity throughout the simulated reactor space. To accomplish this, each entity randomly selects a different vector length and direction (bounded by the reactor dimensions) to move along in each step of the simulation. As a baseline, a speed of approximately 590 nm/s (plus or minus slight random noise) (Pogson et al., 2006) was used to maintain proper mixing of entities in the simulated reactor space. A sparse lattice is used to track the location of all chemical entities throughout the simulation as a way to reduce the memory footprint of the model by avoiding the performance penalties of tree-based spatial datasets due to mutability and the constant updating required for entity movement and chemical reactions. The sparse lattice is divided into two parts: (1) the chemical entity's location in space, and (2) the entity's relationship with others. An overall procedure is shown in Fig. 1.

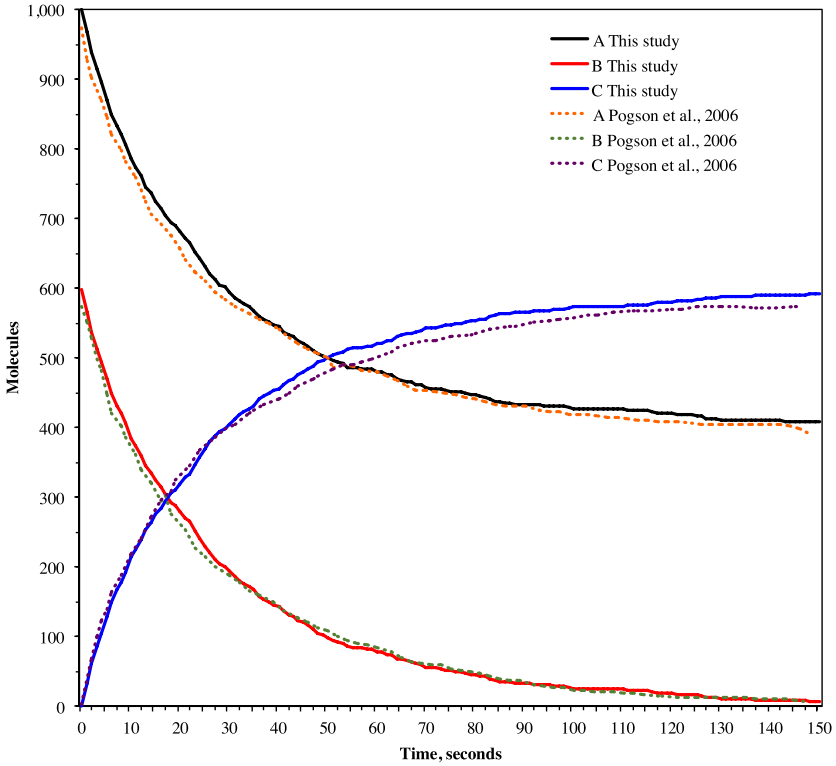

Fig. 2. Comparison of time-dependent molecules of A, B, and C between the result by (Pogson et al. (2006)) and this study.

2.2.3. Elementary reaction mechanisms and reaction rate constants

Table S1 in supplementary material (SM) lists all the elementary reactions and rate constants used in the simulation of acetone degradation in UV/H_2O_2 AOP. The detailed treatment of each reaction mechanism in our ABM is explain below.

Our experimental observations indicate that the decay of H_2O_2 follows between 0th- and 1st-order kinetics in response to both UV photolysis and subsequent reactions of other radical species (e.g., $HO_2^{\bullet}/O_2^{\bullet-}$). Given that our goal was to simulate the time-dependent profiles of transformation products and that simulating the movement and photochemical reactions of individual photons was beyond the scope of our work, we used a probability function derived from our experimental observations to simulate the decay of H_2O_2 in our ABM.

Bimolecular reactions occur in our ABM with a probability proportionate to experimentally observed reaction rate constants when two reactant entities share the same lattice location in our simulated reactor. Because aqueous-phase second-order reaction rate constants of radical-involved reactions (i.e., $HO^{\bullet}$, disproportionation of peroxyl radicals, $HO_2^{\bullet}/O_2^{\bullet-}$) are close to the diffusion-limit and our ABM already simulates the diffusion contribution of overall reaction rate constant, k, via the movement of simulated chemical species throughout our reactor, it was necessary to use Eq. (10) to isolate the chemical reaction contribution, k_{chem}, of k to determine the probability of a bimolecular reaction in our ABM. Diffusion rate constants, k_{diff}, were calculated using the Smolucowski's equation (von Smoluchowski, 1917).

$$k_{chem} = \frac{k \times k_{diff}}{k + k_{diff}} \tag{10}$$

This approach allows the simulated biomolecular reaction to occur within the designated Δt while incorporating all underlying kinetics.

For the appropriate simulated chemical entities that have not already undergone photolysis or were not part of a bimolecular reaction in a given time-step, unimolecular decay (i.e., H-shift and β-session of alkoxyl radicals) can occur in our ABM in the form of either hydrolysis or the addition of molecular oxygen to carbon-centered radicals available as water/dissolved oxygen in our simulated reactor environment. Since unimolecular reactions in our ABM occur within the Δt of our simulated time-step, we simply replaced the simulated chemical species undergoing unimolecular decay with its simulated product to model this reaction.

Acid-base reactions were designated to occur at the end of each time step in serial fashion because these chemical entities must be determined before they are updated. The number of chemical entities is then adjusted as needed by removing, or adding, entities at random locations to ensure a well-mixed solution.

2.3. Computational resources and source codes

The ABM was developed in Java 8 and contains some source code from the MASON Multiagent Simulation Toolkit (Luke et al., 2005). The Xoroshiro128+ pseudo-random number generator (Blackman and Vigna, 2018) in the DSI Utilities library (Vigna, 2020a) was used for high performance random number generation. Additionally, fastutil (Vigna, 2020b) was used for pre-allocated, high performance hash maps. The source code for the simulation is available on GitHub under an MIT license at https://github.com/forestsim-mtu/chemsim

3. Results and discussion

3.1. Verification of agent-based model

To verify our ABM, we first simulated a generic reaction and compared the resulting time-dependent concentration profiles of each species to those obtained in a previously published model.[13]

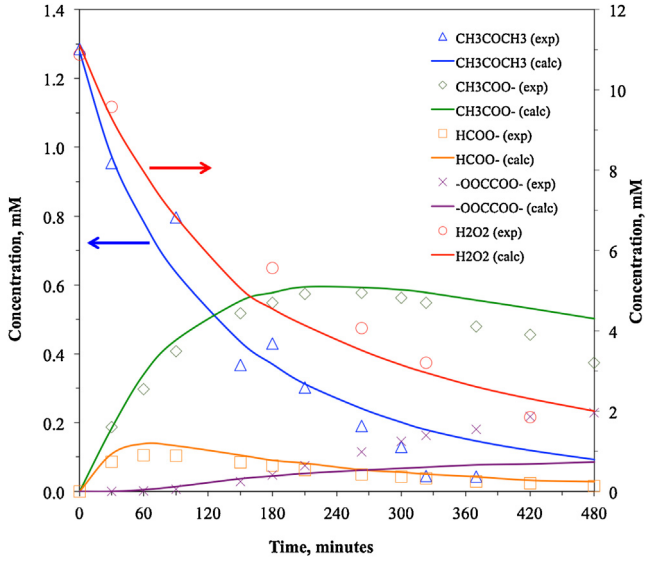

Fig. 3. Time-dependent concentration profiles of H_2O_2, acetone, and major transformation products obtained by our experimental measurements and predicted by ABM.

We simulated the generic reaction A + B → C with a second-order reaction rate constant of 10^6 $M^{-1}s^{-1}$. Our simulated reactor volume was 1 L with initial concentrations of 50 nM of A (i.e., 1,000 entities) and 30 nM of B (i.e., 600 entities). Fig. 2 shows our simulated results in comparison to those obtained in Pogson et al. 2006.[13] While Pogson et al. used matrix operations to determine which agent underwent a reaction as well as to simulated bulk movement operations, our ABM uses a serial approach to agent operations. Sample deviation (SD) values from Eq. (11) were calculated to evaluate any discrepancies between the results of our two models (SD_A = 0.024, SD_B = 0.140, and SD_C = 0.039). This consistency between the predicted profiles of our ABM and that of Pogson et al.[13] verifies that the general reaction kinetics of our model were appropriately implemented

$$SD = \sqrt{\left(\frac{1}{N_i - 1}\right)\sum_{j}^{N_i}\left[\frac{\left(C_{exp,j} - C_{calc,j}\right)}{C_{exp,j}}\right]^2} \quad (11)$$

where N_i is the total number of data points for species i, and $C_{exp,j}$ and $C_{calc,j}$ are the experimental and calculated concentration for species j, respectively. (Fig. 2)

3.2. Overall results

To validate our ABM, we compared the result of a simulated reaction with a parent compound of acetone to the same reaction obtained through our own experimental observation in the laboratory. Fig. 3 displays the time-dependent concentration profiles of H_2O_2, acetone, acetate (CH_3COO^-), formate ($HCOO^-$), and oxalate ($^-OOCCOO^-$) obtained by our experimental measurements and predicted by ABM. The SD values calculated using Eq. (11) were 0.16 for H_2O_2 (0.23 of SD value obtained by ODEs-dependent kinetic model[11]), 0.72 for acetone (0.35), 0.13 for acetate (0.28), 0.32 for formate (0.51), and 0.75 for oxalate (0.52). With the exception of our predicted concentration profiles for acetone and oxalate, the resulting SD values of our ABM were found to be superior to those obtained in our prior research that used an elementary-reaction based kinetic model to solve ODEs numerically. The higher SD

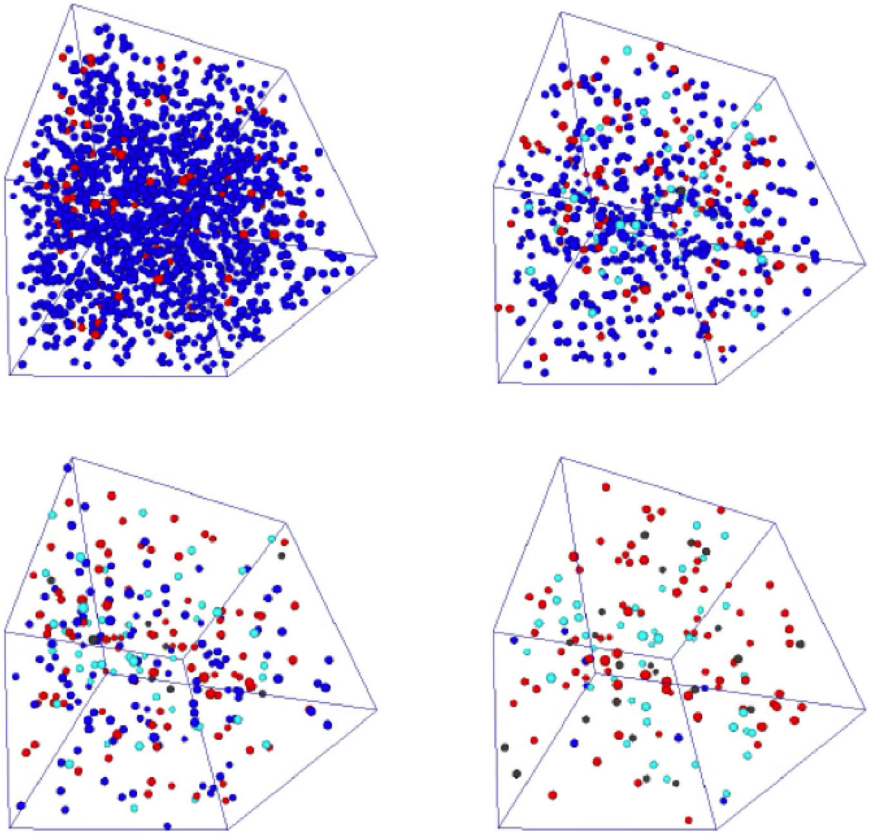

Fig. 4. Snapshots of chemical entities present at different time steps (H_2O_2 in blue, acetone in teal, hydroxyl radicals in red, and a byproduct in dark gray) (For interpretation of the references to colour in this figure legend, the reader is referred to the web version of this article).

value of our ABM-predicted acetone concentration profile appears to be due to the under-prediction of experimentally observed acetone decay after 300 min. This under-prediction of acetone at later points in the simulation occurred because the production of $HO^{\bullet}$ in our ABM results from the H_2O_2 decay at the constant rate that was adjusted with the experimental one. The experimental decay of H_2O_2 apparently follows 0th order at the earlier stage followed by 1st-order at the later stage. Less available H_2O_2 at the later stage caused the less production of $HO^{\bullet}$, which caused the under-prediction of acetone. The same cause seemed to happen for the under-production of oxalate. Elimination of the final two data points from our acetone profile would reduce the SD value to 0.26. Fig. 4 demonstrates the snapshots of chemical entities present at different time steps (note that for simplicity only H_2O_2, acetone, and a byproduct are shown in the defined space). An animation video is available in Fig. S1 in SM.

3.3. Impact of photochemical reactions to the predicted concentration profiles

Unlike ODE-based kinetic models, the number of simulated chemical entities and their distribution in space at any given time-step greatly impacts the predicted concentration profiles of our ABM, as is true for benchtop photo-reactors. Therefore, it is necessary to perform sensitivity analysis to determine the extent to which our results are sensitive to each simulated reaction mechanism and its associated reaction rate constant. The elementary reaction pathways and rate constants used in our ABM were derived from *ab initio* quantum mechanical calculations performed on our previously developed elementary reaction-based kinetic model for the fate of acetone and some reaction rate constants were adjusted with the concentration profile obtained by experiment in this study (Table S1 of SM). A few rate constants were adjusted with the experimentally obtained reaction rate constants (Table S1 of SM), although the adjusted rate constants were not significantly different from those that were reported by experiments. Our ABM simulates the photochemical reactions of photolysis, bimolecular reactions, unimolecular decay, and acid-base dissociation reactions in order within the context of a serial computing environment. This order of operations prioritizes low probability reactions (i.e., photolysis and bimolecular reactions) over high probability reactions (i.e., unimolecular decay and acid dissociation) to ensure all reactions are executed. Acid-base dissociation reactions are then executed at the end of each time step so that the total number of molecules (or chemical entities) is available at the beginning of the next time-step necessary for accounting calculations to be performed. Below, we evaluate and discuss the sensitivity of the predicted concentration profiles from above to each simulated reaction mechanism and highlight the results from the analysis of representative compounds.

Sensitivity analysis revealed that the *k* value used to simulate bimolecular reactions in our ABM significantly impacts the time-dependent profiles of its associated species (i.e., acetone, CH^3COO^-, $HCOO^-$). To conduct this analysis, we reran our simulation using the same initial conditions while incrementally adjusting our reaction rate constant (or the probability of a biomolecular reaction) within a difference of factor of two and 0.5, which is in line with the maximum uncertainty of difference factor of experimentally measured rate constants. Fig. 5 shows the resultant profiles of acetone, CH_3COO^-, and $HCOO^-$ in response to this manipulated k value. Full sensitivity analysis results are provided in SM.

3.4. Limitations of ABM and environmental implication

This study shows how the novel approach of ABM simulation can be used to predict the fate of degradation products of organic

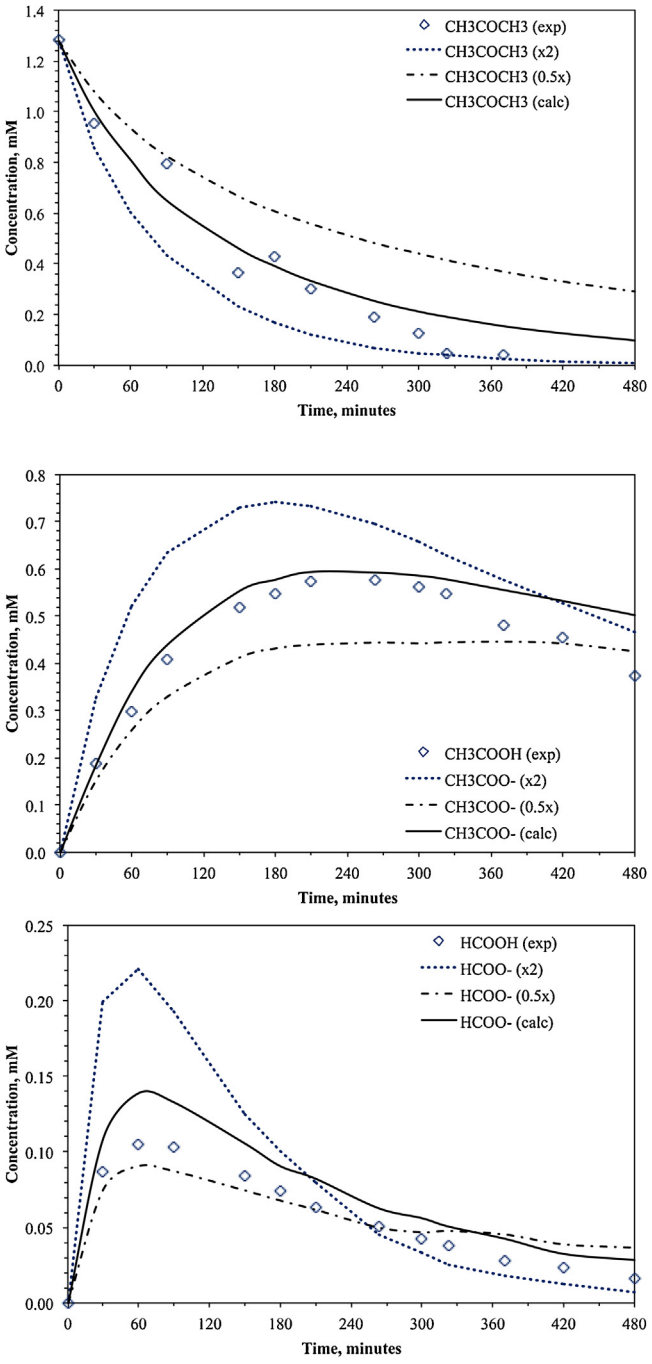

Fig. 5. Sensitivity analysis results for acetone, acetate, and formate.

compounds in UV/H_2O_2 AOP. Our ABM was developed based on the local interaction method of Pogson et al. (2006) and successfully applied to large-scale chemical reactions. This approach is valuable for applications to complex radical-involved physical chemical reactions in other environmental media, such as atmosphere and natural aquatic environment, that greatly challenge the ability of conventional ODE-based kinetic models to produce numerical solutions. Although our ABM is limited in the sense that it is built upon the simplified concept of spherical interaction and it does not simulate micro-mixing or the movement of photons from a UV lamp, we have shown that our approach can produce results in a way that better informs our understanding of the micro-level dynamics underlying molecular interactions, re-activities, and byproduct formation than traditional ODE-based kinetic models.

Supplementary material

Detailed descriptions of experiments, ABM development, simulation procedures, are available in Text in SI, verification result, full list of reaction pathways, and sensitivity analysis results are also available in Figures and Tables in SI.

Declaration of Competing Interest

The authors declare that they have no known competing financial interests or personal relationships that could have appeared to influence the work reported in this paper.

Acknowledgements

This work was supported by the National Science Foundation Award: CBET-1435926. Any opinions, findings, conclusions, or recommendations expressed in this publication are those of the authors and do not necessarily reflect the view of the supporting organization. E.C. appreciated the supports from AWWA through 2018 Carollo/Bryant L. Bench Scholarship and Michigan Space Grant Consortium fellowship.

Appendix A. Supplementary data

Supplementary material related to this article can be found, in the online version, at doi:https://doi.org/10.1016/j.psep.2020.01.023.

References

Bachman, J.A., Sorger, P., 2011. New approaches to modeling complex biochemistry. Nat. Methods 8 (2), 130–131.
Blackman, D., Vigna, S., 2018. Scrambled linear pseudorandom number generators. ArXiv E-Prints, arViv, 1805.01407.
Buxton, V.B., Greenstock, C.L., Helman, W.P., Ross, A.B., 1988. Critical review of rate constants for reactions of hydrated electrons, hydrogen atoms and hydroxyl radicals (•OH/•O-) in aqueous solution. J. Phys. Chem. Ref. Data 17 (2), 513–795.
Crittenden, J.C., Hu, S., Hand, W.D., Green, A.S., 1999. A kinetic model for H2O2/UV process in a completely mixed match reactor. Wat. Res. 33 (10), 2315–2328.
Glaze, W.H., Kang, J.W., 1989. Advanced oxidation processes. Test of a kinetic model for the oxidation of organic compounds with ozone and hydrogen peroxide in a semibatch reactor. Ind. Eng. Chem. Res. 28, 1580–1587.
Glaze, W.H., Kang, J.W., Chapin, H.D., 1987. The chemistry of water treatment processes involving ozone, hydrogen peroxide and ultraviolet radiation. Ozone. Sci. Eng. 9, 335–352.
Guo, X., Minakata, D., Crittenden, J., 2014. Computer-based first-principles kinetic monte carlo simulation of polyethylene glycol degradation in aqueous phase UV/H2O2 advanced oxidation process. Environ. Sci. Technol. 48 (18), 10813–10820.
Heidler, J., Halden, R.U., 2008. Meta-analysis of mass balance examining chemical fate during wastewater treatment. Environ. Sci. Technol. 42 (17), 6324–6332.
Heyes, T.B., Khoury, V., Narayan, A., Nazir, M., Park, A., Brown, T., Adame, L., Chan, E., Buchholz, D., Stueve, T., Gallipeau, S., 2010. Atrazine induces complete feminization and chemical castration in make African clawed frogs (Xenopus laevis). PNAS 107 (10), 4612–4617.
Kamath, D., Mezyk, S., Minakata, D., 2018. Elucidating the elementary reaction pathways and kinetics of hydroxyl radical induced acetone degradation in aqueous phase advanced oxidation processes. Environ. Sci. Technol. 52 (14), 7763–7774.
Klann, M.T., Lapin, A., Reuss, M., 2011. Agent-based simulation of reactions in the crowded and structured intracellular environment: influence of mobility and location of the reactants. BMC Syst. Biol. 5, 71–85.
Kolpin, D.W., Furlong, E.T., Meyer, M.T., Thurman, E.M., Zaugg, S.D., Barber, L.B., Buxton, H.T., 2002. Pharmaceuticals, hormones, and other organic wastewater contaminants in U.S. streams, 1999-2000: a national reconnaissance. Environ. Sci. Technol. 36, 1202–1211.
Luke, S., Cioffi-Revilla, C., Panait, L., Sullivan, K., Balan, G., 2005. MASON: A multiagent simulation environment. Simulation 81 (7), 517–527.
NRC, 2012. Water Reuse Potential for Expanding the Nation's Water Supply Through Reuse of Municipal Wastewater. The national academy press, Washington D.C.
Peyton, G.R., 1990. Guidelines for the Selection of a Chemical Model for Advanced Oxidation Processes. Proceedings of a Symposium on Advanced Oxidation Processes for the Treatment of Contaminated Water and Air, June 4 and 5.
Pogson, M., Smallwood, R., Qwarnstrom, E., Holcombe, M., 2006. Formal agent-based modelling of intracellular chemical interactions. BioSystems, 37–45.
Vigna, S., 2005. DSI Utilities Version 2.5.4. Universita degli Studi di Milano, Milan, Italy http://dsiutils.di.unimi.it/.
Vigna, S., 2018. DSI Fastutil Version 8.2.2. Universita degli Studi di Milano, Milan, Italy http://dsiutils.di.unimi.it/.
von Smoluchowski, M., 1917. Versuch eine mathematicschen Theorie der Koagulationskinetick kolloidaler Losungern. Z. Phys. Chem. N. (N F) 92, 129–168.
Westerhoff, P., Yoon, Y., Snyder, S., Wert, E., 2005. Fate of endocrine disruptor, pharmaceutical, and personal care product chemicals during simulated drinking water treatment processes. Environ. Sci. Technol. 39, 6649–6663.